

by D. C. Kammer and M. J. Triller, University of Wisconsin

# ABSTRACT

A method is presented for target mode identification and sensor placement on a phase-by-phase basis for sequentially assembled large space structures. At each phase, a Craig-Bampton representation is generated by constraining the structure at the actuator locations and at the interface to the next phase. Fixed interface modes are computed and ranked according to dynamical importance using an absolute measure called effective excitation mass. Modes with large excitation mass are strongly excited by the actuators during a current phase modal survey, or will be strongly excited by inputs from the next-phase structure. Inclusion of fixed interface modes in the Craig-Bampton representation which are strongly excited by the next-phase structure allows sensors placed during the current phase to do a better job of anticipating the dynamics which will be important in the next phase. Finite element model modes which are accurately predicted by the Craig-Bampton representation are used as target modes for sensor placement. Sensors are placed such that the target mode partitions are as spatially independent as possible. In a numerical example, the sensor configurations placed using the proposed method provided superior Fisher Information matrix determinants and condition numbers for initial and intermediate phases when compared to results using sensor configuration subsets placed optimally for the full structure.

$[A_f]$ information matrix	$[K_{ff}]$ stiffness matrix for fixed interface system with rigid body modes constrained
$[C]$ cross-orthogonality matrix	$[M]$ physical mass matrix
$[E]$ effective mass matrix	$[M_{CB}], [K_{CB}]$ Craig-Bampton representation mass and stiffness matrices
$[E_{CB}]$ normalized effective mass matrix	$[M_\psi]$ constraint mode mass matrix
$\{E_D\}$ Effective Independence distribution vector	$[P]$ estimate error covariance matrix
$\{F\}$ applied force vector	$[P_r], [P_e]$ projector matrices
$[G_{ff}]$ flexibility matrix associated with $K_{ff}$	$\{q\}$ modal displacement vector
$[G_{oo}^e]$ flexibility matrix corresponding to elastic fixed interface modes	$[Q]$ Fisher Information matrix
$[I]$ identify matrix	$[R]$ noise covariance intensity matrix
$[K]$ stiffness matrix	$[T]$ transformation matrix

Dr. Daniel C. Kammer (SEM member), Assistant Professor, and Michael J. Triller, Graduate Student, Department of Engineering Mechanics, University of Wisconsin.

Final manuscript received: January 14, 1992



$\{u\}$	displacement vector	<b>Subscripts</b>	
$\{u_{CB}\}$	Craig-Bampton displacement vector	$a$	matrix partitions corresponding to $a$ -set
$\{v\}$	noise vector	$o$	matrix partitions corresponding to $o$ -set
<b>Greek</b>		$s$	matrix partitions corresponding to sensor locations
$[\Phi]$	elastic mode shapes	<b>Superscripts</b>	
$[\Phi_r]$	rigid body mode shapes	$T$	denotes transpose
$[\Phi_o']$	fixed interface rigid body modes	$\wedge^2$	term by term matrix multiplication
$\{\psi\}, \lambda$	eigenvectors and eigenvalues of information matrix		
$[\Psi_o]$	constraint mode matrix		

Accurate analytical models will be required for structural dynamic analysis, control system design, and health monitoring of proposed large space structures. Test-analysis correlation [1,2] and model updating techniques [3-5] must be used to identify and correct inaccuracies in the analytical models representing these structures such that they accurately predict modal parameters determined during modal surveys. Due to size, flexibility, and the inability to accurately simulate a zero-g environment, a ground vibration test of a complete large space structure is not possible. Therefore, these structures must be tested on-orbit. This presents many difficulties that are not apparent during a ground vibration test.

A key problem in on-orbit modal identification is the placement of sensors. In the case of a ground vibration test, the structure can be literally plastered with a large number of sensors. If the appropriate data is not being obtained during the course of the test, sensors can be moved with relative ease. However, in the case of an on-orbit test, the number of sensors will be extremely limited due to weight and cost considerations. Once the structure is placed in orbit, sensors will be difficult if not impossible to move. Therefore, the small allotted number of sensors must be placed on the structure to identify a limited number of dynamically important target modes. A systematic approach must be used to place the sensors in an optimal sense especially in the case of large space structures where there are usually a very large number of responding mode shapes with closely spaced frequencies.


While many authors have considered sensor placement for control purposes [6-9], a relatively small number have considered sensor location in structural identification [10,11]. Only Refs. [12-16] have considered sensor placement for modal identification from the standpoint of a structural dynamicist who must use test data to perform test-analysis correlation for analytical model updating. The modal partitions obtained from the test data must be linearly independent otherwise correlation and model updating analysis will fail because the test mode shapes will not be spatially discernible. It has also been shown that spatial independence of the target mode partitions yields improved modal identification results [16]. In general, spatial independence is not a problem in the case of a ground vibration test where a very large number of sensors is used. However, when only a limited number of sensors is available, care must be taken to place them properly.

In addition, there is a characteristic unique to large space structures which has not yet been considered in the context of sensor placement. That is, proposed large space structures will be assembled and identified in a sequential fashion. After each phase is completed, an on-orbit modal identification will be performed for the purpose of structural analysis and control. The sensor configuration for each phase must be capable of identifying the current target modes, but it must also be capable of contributing in an efficient manner to the identification of the target modes of the next phase. In some sense, efficiency or optimality of the



sensor configuration must be maintained over all phases of the structure until completion such that sensor resources can be conserved.

This paper presents a systematic method for placing sensors in an efficient manner during the sequential construction of a large space structure. The approach will use a previously developed method of sensor placement [12, 14], called Effective Independence, and substructure representations in conjunction with a measure of modal dynamic importance to place sensors in anticipation of sequential assembly. The measure of dynamic importance presented in this paper represents a novel nonstandard application of the well known effective mass [1] measure to select target modes for an unconstrained structure which will be strongly excited by actuators and interface loads during an on-orbit test. A simple numerical example will be used to demonstrate the theory developed in the paper.



The idea behind the method presented here is to place a small number of sensors on each construction phase of the large space structure which will obtain measurements that spatially differentiate the mode shapes that are strongly excited by actuators during the current phase. In addition, the same sensor set must be able to anticipate modal participation due to inputs from the adjacent structure to be attached in the next phase. Excepting the case of the final completed structure, the set of target modes for each phase is thus the union of two subsets consisting of modes excited by actuators and modes which will be excited by future input from adjacent substructure. This target mode set must first be identified and then sensors must be placed such that the target modes are spatially differentiated. It is believed that if target modes are selected correctly, the majority of sensors placed for the current phase will still contribute significantly in future phases. It is important to note that in the theory and analysis presented in this paper, it is assumed that the actuator locations have been selected such that system modes which are important for model updating, health monitoring, etc., are strongly excited. The strongly excited modes, or target modes, thus coincide with mode shapes which are of importance in post-test analysis.

### **(a) Selection of Target Modes**

In order to accomplish the desired objective, an appropriate measure of modal dynamic importance must be developed. This measure will be used to identify target modes which must be spatially discernible during each structure phase. Closely related to this topic, a vast amount of research has been devoted by the control dynamics community to the reduction of analytical models for use in control system design and simulation. Proposed methods include Internal Balancing [17], Optimal Projection [18], Modal Cost [19], as well as many others. Each of these methods determines the dynamic importance of individual system mode shapes and then uses this ranking to eliminate unimportant modes from the analytical representation. These modal ordering techniques are based upon measures of controllability and observability which are derived from the actuator/sensor configuration.

Controllability can be used to rank the dynamic importance of each mode based on the chosen actuator set. The larger the measure of controllability, the less effort is required to control or excite the mode. However, controllability, as defined by the control dynamics community, is only a relative measure of importance. It can only be said that one state is important relative to another and this measure of importance may have no physical significance from the structural dynamics point of view. In contrast, structural dynamicists measure the dynamic importance of each generalized coordinate in a modal space using the effective mass matrix [1,20] given by



$$[E] = ([\Phi]^T [M] [\Phi_r])^2 \quad (1)$$

where  $[\Phi]$  are the elastic mode shapes of the system,  $[M]$  is the physical mass matrix,  $[\Phi_r]$  is a set of rigid body modes, and the symbol  $()^2$  denotes a term by term multiplication. The effective mass is a measure of the amount of mass in each mode shape participating in each of the six rigid body directions. Unlike controllability, the effective mass is an absolute measure of dynamic importance. As more elastic modes are added to the computation, the sums of the columns of the effective mass matrix approach the rigid body mass and inertia values. The effective mass is actually a measure of the completeness of the set of elastic mode shapes retained in the analysis. If the retained modes have a combined effective mass of at least 90% over all of the rigid body directions, it is standard practice to assume that all of the dynamically important modes are included in the elastic mode set.

Unfortunately, the effective mass is identically zero for free-free systems, therefore the measure cannot be directly used in the case of large space structures. However, an alternative coordinate space can be examined by transforming the system to a Craig-Bampton representation [21] which includes a set of elastic fixed-interface modes possessing nonzero effective mass. For each phase of the construction, the physical degrees of freedom of the corresponding finite element model are partitioned into two complimentary sets  $a$  and  $o$ , where the  $a$ -set includes all degrees of freedom at the actuator locations for the current phase and at the interfaces with structure which will be added for the next phase. Note that the actuator and next-phase interface locations are not necessarily the same. This partitioning results in an equation of motion for the free-free structure of the form

$$\begin{bmatrix} M_{oo} & M_{oa} \\ M_{ao} & M_{aa} \end{bmatrix} \begin{Bmatrix} \ddot{u}_o \\ \ddot{u}_a \end{Bmatrix} + \begin{bmatrix} K_{oo} & K_{oa} \\ K_{ao} & K_{aa} \end{bmatrix} \begin{Bmatrix} u_o \\ u_a \end{Bmatrix} = \begin{Bmatrix} 0 \\ F_a \end{Bmatrix} \quad (2)$$

where it has been assumed that loads are applied only at the actuator and interface locations. If the  $a$ -set degrees of freedom are sufficient to fully constrain the structure, the upper partition of the static portion of Eq. (2) can be solved to determine the  $o$ -set displacement in terms of the displacement of the actuator/interface set yielding

$$\{u_o\} = -[K_{oo}]^{-1} [K_{oa}] \{u_a\} = [\Psi_o] \{u_a\} \quad (3)$$

Constraining the actuator and interface displacements to zero, the corresponding  $o$ -set eigenvalue problem can be solved to yield a set of fixed-interface elastic modes  $[\Phi_o]$ . The results of Eq. (3) and the fixed-interface modes can be combined into a set of displacement vectors which can be used to generate a transformation from the original physical configuration space of the finite element model  $u$  to the Craig-Bampton hybrid coordinate space  $u_{CB}$

$$\{u\} = \begin{bmatrix} \Phi_o & \Psi_o \\ 0 & I \end{bmatrix} \begin{Bmatrix} q \\ u_a \end{Bmatrix} = [T] \{u_{CB}\} \quad (4)$$

The first column partition of  $[T]$  contains the fixed-interface modes which describe the system dynamics relative to the current-phase actuators and the next-phase interface. The second partition of columns are static shapes called constraint modes [21]. In the sequel, these static shapes will be referred to as excitation constraint modes. Each column represents the deformation of the structure when the corresponding actuator or interface location is given a unit displacement with all of the remaining actuator/interface locations fixed. The coordinate space of the Craig-Bampton representation contains the physical



displacements of the actuator and interface locations  $u_a$  and the modal displacements of the fixed-interface modes  $q$ .

In the application of the Craig-Bampton representation to each construction phase of a large space structure, a special case can arise in which the actuator and next-phase interface degrees of freedom are not sufficient to fully constrain the structure. The situation is more common for the last phase or full structure where there are only actuator locations and no next-phase interface degrees of freedom. For example, there are plans to perform on-orbit modal identification of Space Station Freedom using its reaction control system (RCS) jets. Fixing the corresponding degrees of freedom in the finite element model will not restrain the longitudinal translation rigid body mode. A straightforward application of the Craig-Bampton representation in this case will not work because the  $o$ -set stiffness partition  $[K_{oo}]$  is singular and thus cannot be inverted to form the constraint modes  $[\Psi_o]$  using Eq. (3). The set of fixed interface modes will now contain rigid body modes corresponding in number to the rank deficiency of  $[K_{oo}]$ .

In order to compute the constraint modes, the flexibility matrix  $[G_{oo}^e]$  corresponding to the elastic fixed interface modes must be computed for the  $o$ -set. This can be accomplished by selecting any set of degrees of freedom from the  $o$ -set which restrain the rigid body modes and then deleting the corresponding rows and columns from  $[K_{oo}]$  resulting in a smaller nonsingular stiffness matrix  $[K_{ff}]$  which can be inverted to form the corresponding flexibility matrix  $[G_{ff}]$ . This matrix is then expanded back to  $o$ -set size by adding the appropriate rows and columns of zeros forming

$$\tilde{G}_{oo} = \begin{bmatrix} G_{ff} & 0 \\ 0 & 0 \end{bmatrix} \quad (5)$$

This  $o$ -set size flexibility matrix now contains a general rigid body displacement which must be removed to form the desired elastic flexibility matrix  $[G_{oo}^e]$ . This can be done by using a spatial filter called an oblique projector [22]. If  $[\Phi_o^r]$  represents the fixed interface rigid body modes, the oblique projector onto the range space of the rigid body modes along the space spanned by the elastic fixed interface modes is given by

$$[P_r] = [\Phi_o^r][\Phi_o^r]^T[M_{oo}] \quad (6)$$

The projector onto the elastic mode space can be computed without calculating all of the elastic fixed interface modes by using the relation

$$[P_e] = [I] - [P_r] \quad (7)$$

The rigid body contribution can be filtered out of Eq. (5) resulting in the desired flexibility matrix using the relation

$$[G_{oo}^e] = [P_e][\tilde{G}_{oo}][P_e]^T \quad (8)$$

The  $o$ -set partition of the corresponding modes is then given by

$$[\Psi_o] = -[G_{oo}^e][K_{oa}] \quad (9)$$

Thus the Craig-Bampton transformation can be applied to represent construction phases of large space



structures in any situation. This approach to finding the flexibility matrix for an underconstrained structure is analogous to the technique used by Rubin [23] to compute residual flexibility.

The mass and stiffness matrices of the finite element representation are transformed to the Craig-Bampton space using the relations

$$[M_{CB}] = [T]^T [M] [T] \quad [K_{CB}] = [T]^T [K] [T] \quad (10)$$

If all of the fixed-interface modes are computed and retained, the finite element and Craig-Bampton representations will be the same size and equivalent. However, the fixed-interface modal coordinates can be ranked by structural importance relative to the inputs using effective mass. Modal coordinates with low effective mass can be eliminated resulting in a reduced representation which is still structurally complete. By including the actuator location degrees of freedom in the  $\alpha$ -set, the effective mass of the fixed interface modes will represent a measure of the excitation of the structure by the actuators during a current-phase modal identification experiment. Including degrees of freedom in the  $\alpha$ -set at interfaces with structure to be added in the next phase will result in the effective mass also being a measure of the excitation of the current-phase portion of the structure during vibrational motion in the next phase.

For the on-orbit excitation problem, the normalized effective mass matrix is computed using the relation

$$[E_{CB}] = \left( [\Phi_{oo}]^T [M_{oo}] [\Psi_o] \right)^2 [diag(M_\Psi)]^{-1} \quad (11)$$

where  $[\Psi_o]$  are the  $\alpha$ -set partitions of the excitation constraint modes, not necessarily rigid body modes as in the usual effective mass computation of Eq. (1), and  $[M_\Psi]$  is the constraint mode mass matrix

$$[M_\Psi] = [\Psi_o]^T [M_{oo}] [\Psi_o] \quad (12)$$

which represents the amount of structural mass affected by each of the actuator and interface inputs. As more fixed-interface modes are included in the representation, the sums of the columns of  $[E_{CB}]$  will approach unity. Each row of  $[E_{CB}]$  represents the contribution of the corresponding fixed interface mode to the total mass influenced by each of the actuators and interface locations. The effective excitation mass vector  $\{E_m\}$  can be computed by adding the columns of  $[E_{CB}]$  and dividing by the number of inputs. Each term in  $\{E_m\}$  represents the fractional contribution of the corresponding fixed interface mode to the structural dynamics excited by the inputs.

If the Craig-Bampton representation is transformed to a state-space form, the work of Ohkami and Likins [24], Likins et. al. [25], and Hughes and Skelton [26] can be used to show that if the fixed interface mode frequencies are not repeated, the  $i$ th fixed interface mode is controllable or excitable by the inputs if and only if its corresponding effective excitation mass  $E_{mi}$  is nonzero. The  $E_{mi}$  value can thus be used as a measure of the mode's excitability. Modes with large  $E_{mi}$  values will be strongly excited by either the actuators of the current phase or inputs from additional structure to be added during the next phase. Unlike the usual relative measures of controllability, effective excitation mass is measured against an absolute value. If enough fixed-interface modes are retained such that their effective excitation mass totals 90% or more of the mass influenced by all of the inputs, the reduced Craig-Bampton transformation will yield an accurate representation of the finite element model for the corresponding actuator and next-phase interface configuration. If fixed interface mode frequencies are repeated, the excitability measure can be easily extended to this case.

The columns of the Craig-Bampton transformation matrix  $[T]$  span the excitable subspace of the original finite element representation of the current phase. The finite element configuration space mode shapes which are strongly excited by the inputs at each phase can be determined by performing an eigenvalue solution using the reduced Craig-Bampton representation and comparing the resulting mode



shapes and frequencies with the finite element model modal parameters using direct comparison and cross-orthogonality checks [1]. The finite element modes which are accurately predicted by the Craig-Bampton representation are the target modes which must be spatially differentiated during each structure phase.

## (b) Placement of Sensors

The Effective Independence sensor placement methodology is described in detail in Refs. [12-14]. A brief summary is presented here for the reader who is unfamiliar with this approach. After the target modes are selected for the current phase of interest, a large set of candidate sensor locations is designated from which the smaller final sensor configuration for the current phase will be selected. Sensor locations which have already been selected for control purposes may also be included in the candidate set to minimize the amount of additional sensor resources required for modal identification. If this is the first phase, any valid sensor locations in the first-phase structure can be placed in the initial candidate set. If subsequent phases are being considered, the initial candidate set must include sensor locations which were selected in previous phases and any valid locations on the new structure added to produce the current phase. The objective of the Effective Independence sensor placement strategy is to select sensor locations which render the target mode partitions as linearly independent as possible while at the same time retaining as much information as possible about the target modal responses within the sensor data.

The sensor placement problem is approached from the standpoint of estimation theory. The target mode independence requirement implies that at any time  $t$ , the sensors can be sampled and the target mode response can be estimated. In the Craig-Bampton space, a static Fisher model [27] is assumed for the output equation of the form

$$\{u_s\} = [\Phi_s]\{q\} + \{v\} \quad (13)$$

in which  $\{u_s\}$  is the response at the sensor locations,  $[\Phi_s]$  are the target modes partitioned to the sensor degrees of freedom,  $\{q\}$  is the target mode response, and  $\{v\}$  is the sensor noise. Assuming  $\{v\}$  to be a stationary additive random observation disturbance with zero mean and positive definite covariance intensity matrix  $[R]$ , an efficient unbiased estimator yields an estimate error covariance matrix of the form

$$[P] = E\left(\left(\{q\} - \{\hat{q}\}\right)\left(\{q\} - \{\hat{q}\}\right)^T\right) = \left([\Phi_s]^T [R]^{-1} [\Phi_s]\right)^{-1} = [Q]^{-1} \quad (14)$$

where  $E$  represents the expectation operator and  $[Q]$  represents the Fisher Information Matrix [28]. Maximization of  $[Q]$  results in the minimization of the error covariance matrix  $[P]$  which results in the best estimate  $\{\hat{q}\}$ .

The derivation of the Effective Independence method presented in Ref. [12] assumes that the sensor noise is uncorrelated and statistically identical for all sensors. Reference [14] extended the method to include a general form for the noise model. The analysis presented in this paper will use the simplified noise representation. Thus the covariance intensity matrix is given by  $[R] = \sigma^2 [I]$  in which  $\sigma^2$  is the sensor noise variance and  $[I]$  is an identity matrix. The Fisher Information Matrix then becomes

$$[Q] = \frac{1}{\sigma^2} [\Phi_s]^T [\Phi_s] = \frac{1}{\sigma^2} [A_f] \quad (15)$$

Maximization of  $[Q]$  results in the maximization of matrix  $[A_f]$  independent of the sensor variance, therefore,  $[A_f]$  will be referred to as the information matrix in the remainder of this paper. The initial candidate sensor set is selected such that  $[\Phi_s]$  is full column rank implying that  $[A_f]$  is positive definite.

The method proceeds by computing the Effective Independence distribution vector  $\{E_D\}$  using the relation



$$\{E_D\} = ([\Phi_s][\psi])^2 [\lambda]^{-1} \{1\}_r \quad (16)$$

where  $[\psi]$  are the orthonormal eigenvectors of positive definite  $[A_f]$ ,  $[\lambda]$  are the corresponding eigenvalues, and  $\{1\}_r$  is a column vector of 1's with dimension  $r$  corresponding to the number of target vectors. Reference [13] illustrated that vector  $\{E_D\}$  is the diagonal of an orthogonal projector [22] onto the range space spanned by the columns of  $[\Phi_s]$ . Terms within  $\{E_D\}$  were shown to represent the fractional contribution of each sensor location to the independence of the target modes. Entries in  $\{E_D\}$  are sorted by magnitude and the lowest ranked sensor which is not a sensor selected from a previous phase is deleted from the candidate set. Remaining sensor locations are then ranked and sorted again. In an iterative fashion, the initial candidate set of sensor locations is rapidly reduced to the number allotted for testing the current phase. The resulting sensor configuration tends to maintain the determinant of the information matrix  $[A_f]$  which leads to a smaller error covariance matrix and better estimates of the target mode response. This determinant is a direct measure of the amount of target modal response information contained in the sensor data [29]. It can be used to determine the goodness of one sensor set with respect to another.

### 3 Numerical Example

A numerical example consisting of a simplified large space structure representation will be used to demonstrate the application of the sensor placement method described in the previous section. The space structure considered is illustrated in Fig. 1. Its motion will be constrained to the  $xy$  plane to further simplify the analysis. The corresponding finite element representation contains 46 grid points, each with  $x$  and  $y$  displacements, resulting in 92 total degrees of freedom. Twenty one grid points are evenly distributed along the length of the main truss while 6 grids are evenly distributed along each of the four photovoltaic (PV) arrays located at the ends of the truss. The main truss structure is 3.5 times the length of the PV arrays. Simple Euler beam elements are used to model the main truss and the arrays. The mass distributions for both the truss and the arrays are even and identical. An additional mass of 0.75 times the main truss mass ( $M_T$ ) is evenly distributed over the central element of the main truss. Concentrated masses of  $0.03 M_T$  are located at each of the PV array tips, while concentrated masses of  $0.19 M_T$  are placed at the end of the truss.

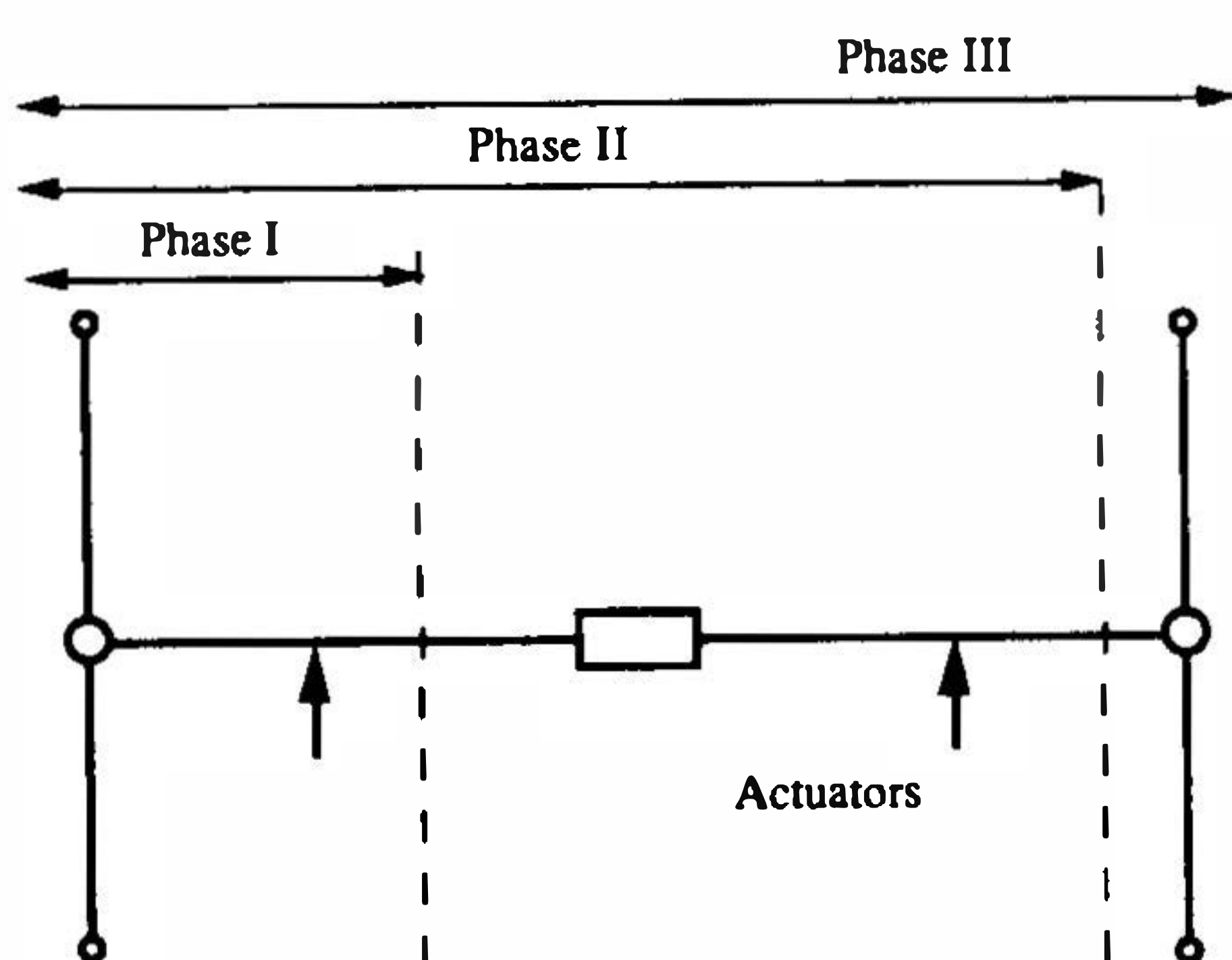


Fig. 1 Simple large space structure representation with three construction phases

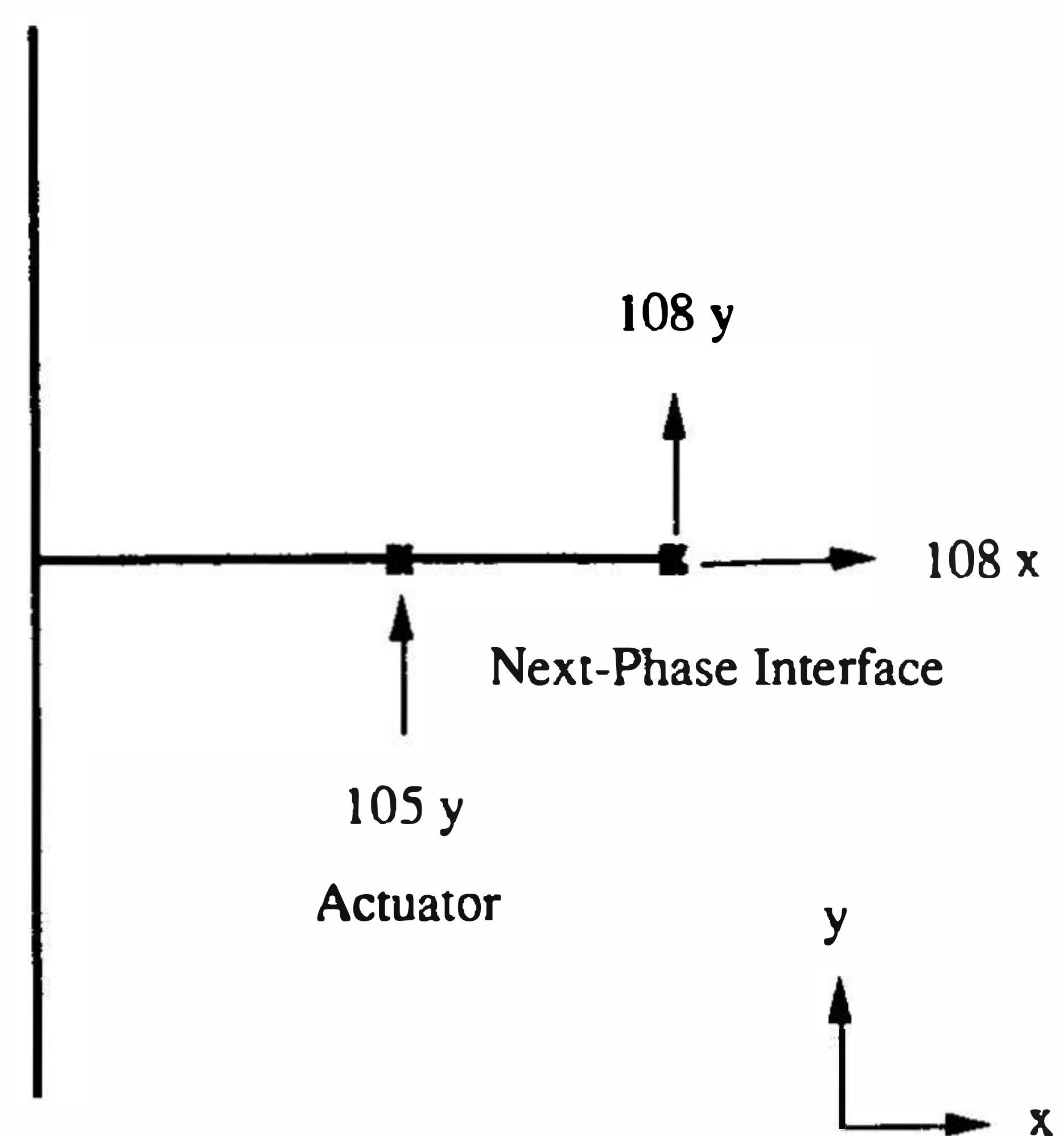


Fig. 2  $\alpha$ -set degrees of freedom for Phase I



The dimensionless parameter  $\beta = EI/L^4m$  for the main truss and PV array finite elements is given by  $\beta_{Truss} = 2.16$  and  $\beta_{PV} = 0.54$ , where  $E$  is the elastic modulus,  $I$  is the area moment of inertia of the beam cross section,  $L$  is the element length, and  $m$  is the mass per unit length. Beam parameters were chosen for the model such that the first several modal frequencies are characteristic of expected large space structure frequencies.

The space structure will be constructed in three phases as pictured in Fig. 1. In the final phase, the structure will be excited for modal identification purposes using the two actuator locations pictured, perhaps these could be RCS jets. These actuator locations will also be used to excite the structure during each phase of construction for modal identification. Starting with the Phase I structure, the Craig-Bampton representation was formed by constraining the actuator location degree of freedom, node 105 in the  $y$  direction, and the degrees of freedom at the interface to the structure which will be added in Phase II, node 108 in the  $x$  and  $y$  directions. These degrees of freedom which make up the  $a$ -set are illustrated in Fig. 2. Fixed interface mode shapes were then computed for the Phase I  $a$ -set degrees of freedom. The  $a$ -set is sufficient to constrain all the rigid body modes therefore no zero frequency modes appear in the fixed interface mode set. Because these modes are constrained, they possess a nontrivial effective excitation mass which is computed by averaging the effective mass matrix of Eq. (11) over each row. The result for the first 30 fixed interface modes is illustrated in Fig. 3. Modes which are significantly excited by the actuator and interface inputs are easily picked out. Table 1 lists the ten most important fixed interface modes based upon their effective excitation mass values. The highest ranked mode is illustrated in Fig. 4. Tracking the cumulative value of the effective excitation mass, Table 1 indicates that retaining 6 fixed interface modes is sufficient to maintain 95% of the Phase I dynamics affected by the actuator/interface inputs.

Augmenting the six selected fixed interface modes with three excitation constraint modes corresponding to the  $a$ -set provides the reduced Craig-Bampton transformation matrix via Eqs. (3) and (4). The Craig-Bampton representation is generated using Eq. (10) and an eigenvalue solution can be performed to produce nine unconstrained modal parameters in the reduced Craig-Bampton configuration space. If the mode shapes are transformed back to the original Phase I finite element model configuration space using the Craig-Bampton transformation, they can be compared with the free-free finite element model mode shapes using the cross-orthogonality computation

$$[C] = [\Phi_{FEM}]^T [M] [\Phi_{CB}] \tag{17}$$

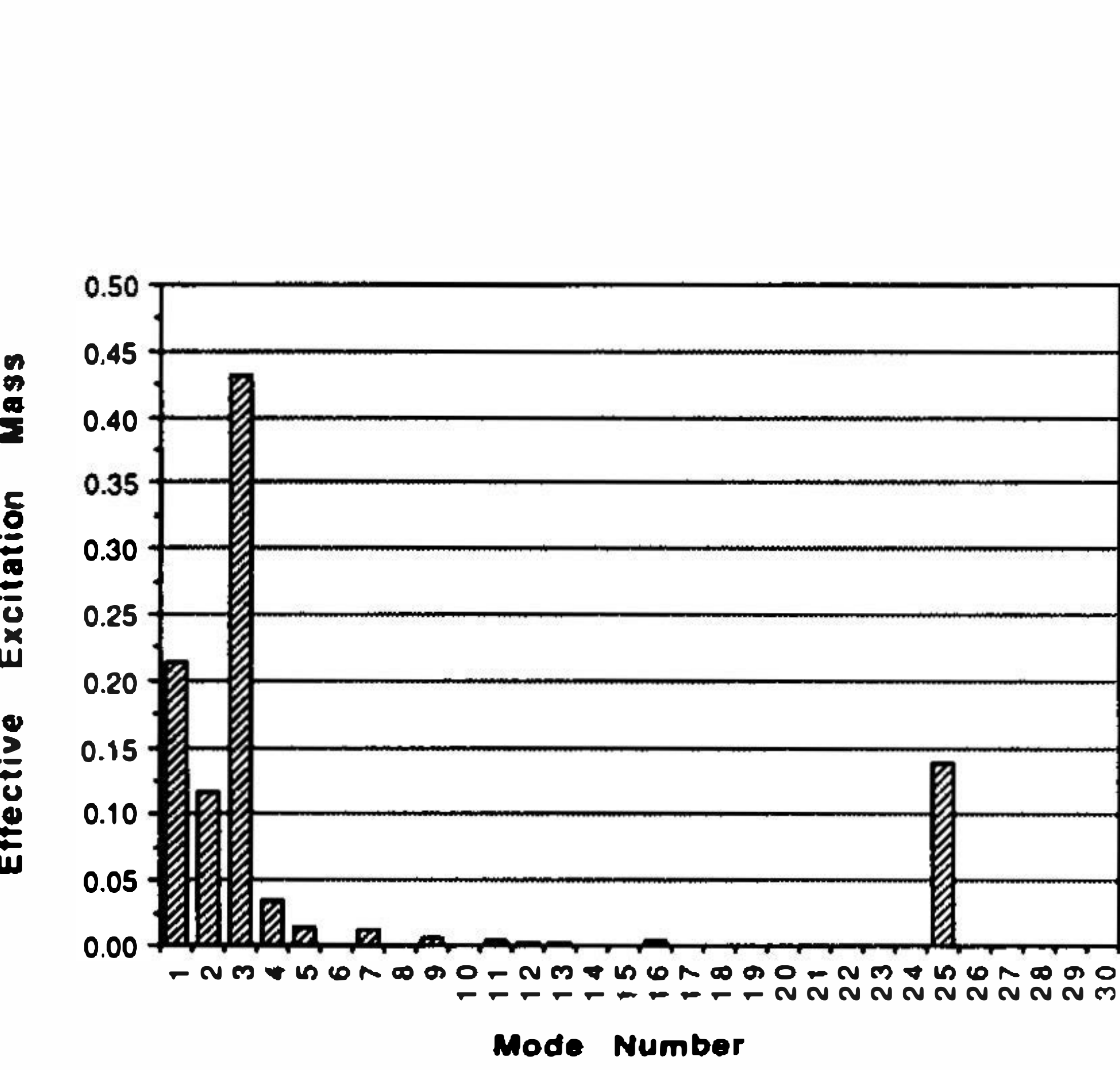


TABLE 1 TEN MOST IMPORTANT PHASE I FIXED INTERFACE MODES BASED ON EFFECTIVE EXCITATION MASS

Mode	Freq. (Hz)	Eff. Mass	Cumulative Eff. Mass
3	0.321	0.431	0.431
1	0.073	0.213	0.644
25	55.500	0.138	0.782
2	0.076	0.117	0.899
4	0.500	0.035	0.934
5	0.505	0.014	0.947
32	199.470	0.012	0.961
7	1.440	0.006	0.973
9	2.899	0.004	0.979
16	11.996	0.004	0.983

Fig. 3 Effective excitaton mass for Phase I fixed interface modes



in which  $[\Phi_{FEM}]$  are the Phase I finite element model mode shape and  $[\Phi_{CB}]$  are the expanded Craig-Bampton representation modes. Assuming that both mode sets are mass normalized, a value of 1.00 at the  $ij$ th entry in the cross-orthogonality matrix  $[C]$  indicates that the  $i$ th finite element model mode shape correlates perfectly with the  $j$ th Craig-Bampton predicted mode shape if all other entries in the  $i$ th row and  $j$ th column are 0.0. Based upon cross-generalized mass (CGM) values and frequency comparisons, seven finite element representation modes were accurately predicted by the Craig-Bampton representation. The results of the correlation are listed in Table 2. Frequency error is less than 0.10% and mode shape error is essentially zero.

The four elastic mode shapes predicted by the Craig-Bampton representation were used as target modes

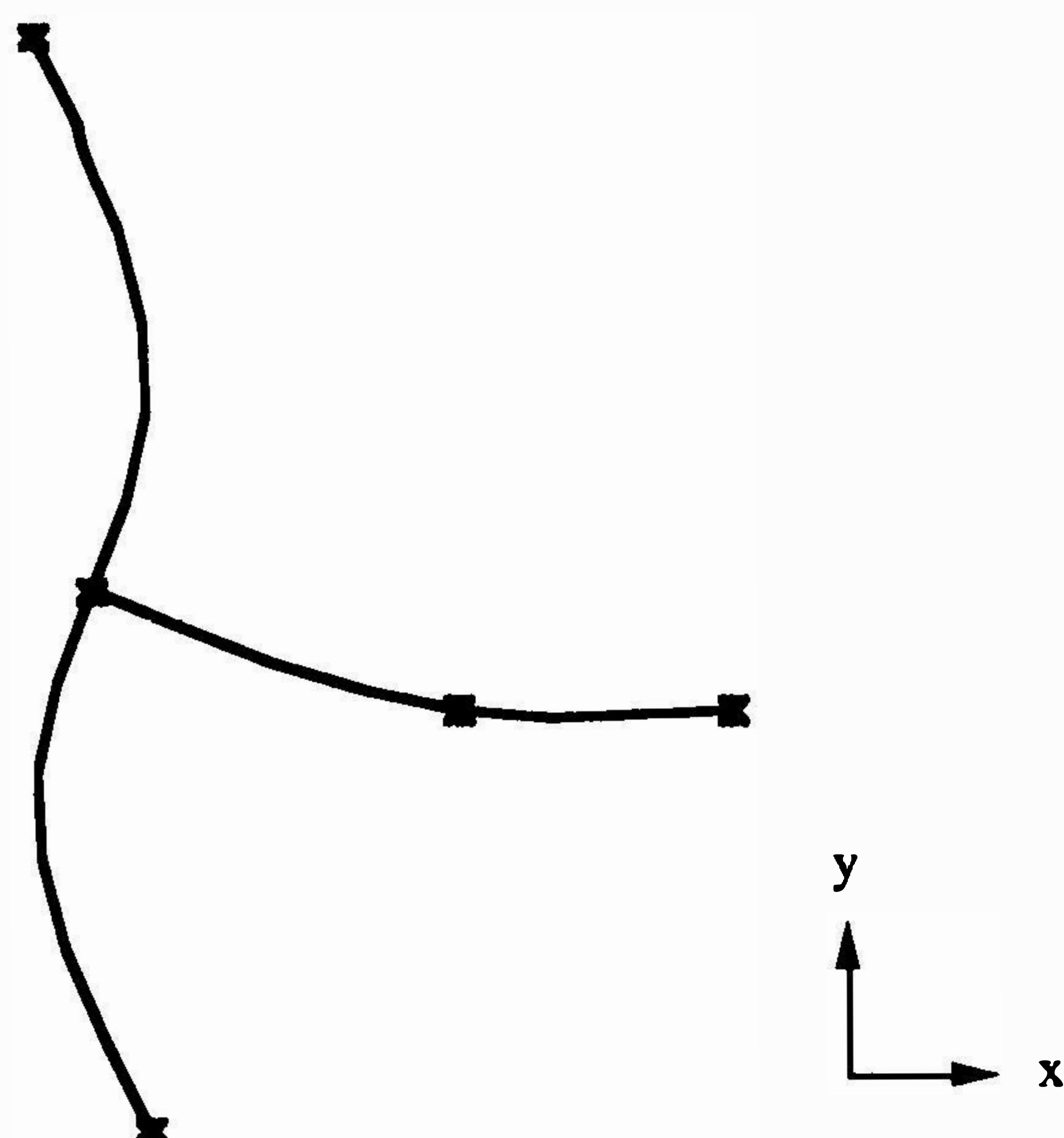


Fig. 4 Fixed Interface mode 3 possess largest effective excitation mass

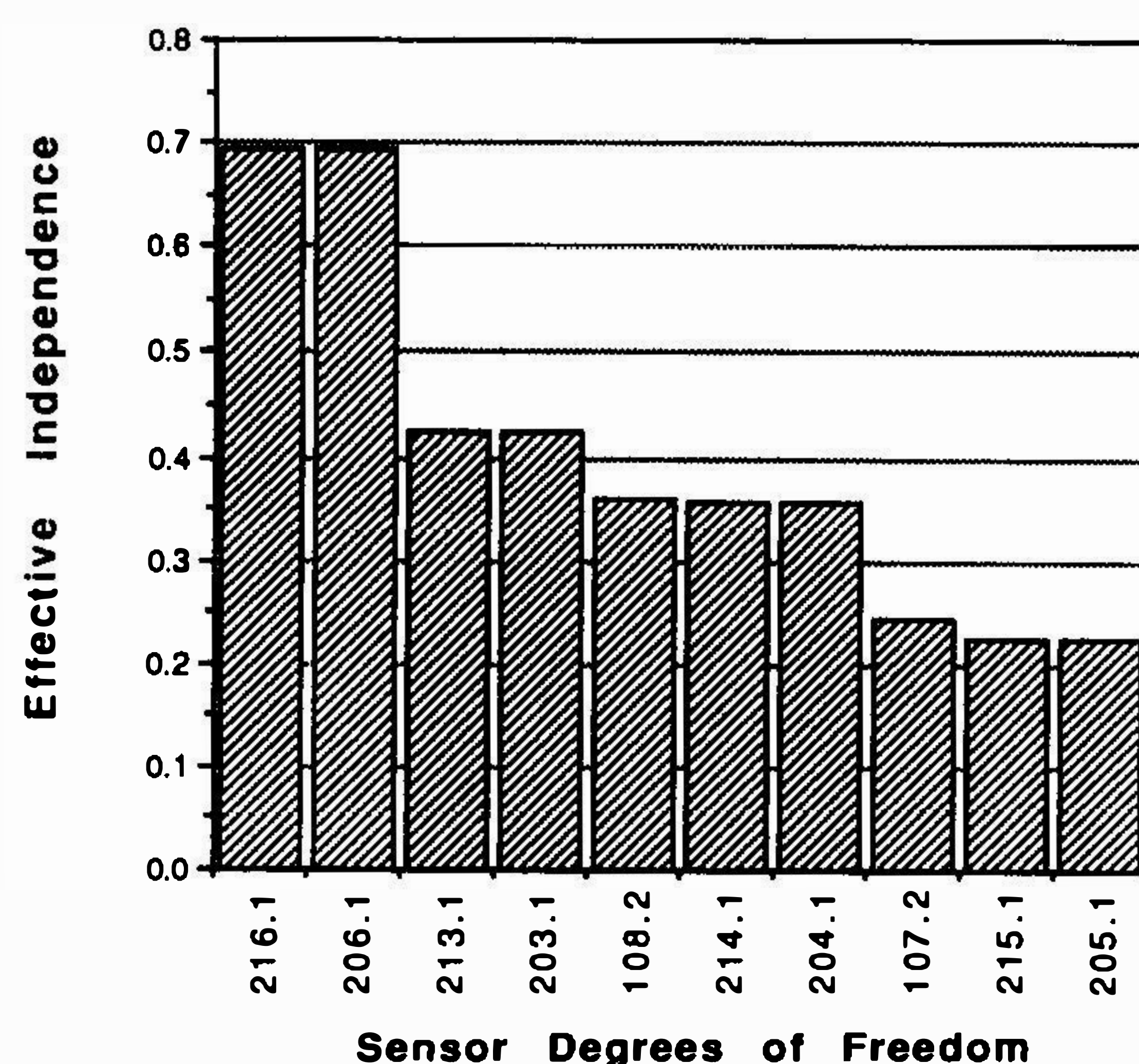


Fig. 5 Effective Independence distribution for Phase I sensor configuration

TABLE 2 FINITE ELEMENT MODEL/CRAIG-BAMPTON REPRESENTATION CORRELATION RESULTS FOR PHASE I

FEM Mode	Freq. (Hz)	CB Mode	Freq. (Hz)	Absolute % Error	CGM
1	0.000	1	0.000	0.000	1.00
2	0.000	2	0.000	0.000	1.00
3	0.000	3	0.000	0.000	1.00
4	0.094	4	0.094	0.004	1.00
5	0.129	5	0.129	0.003	1.00
6	0.505	6	0.505	0.003	1.00
7	0.544	7	0.544	0.093	1.00
9	1.488	9	107.010	7093.500	0.83
10	2.641	8	2.785	5.420	0.42

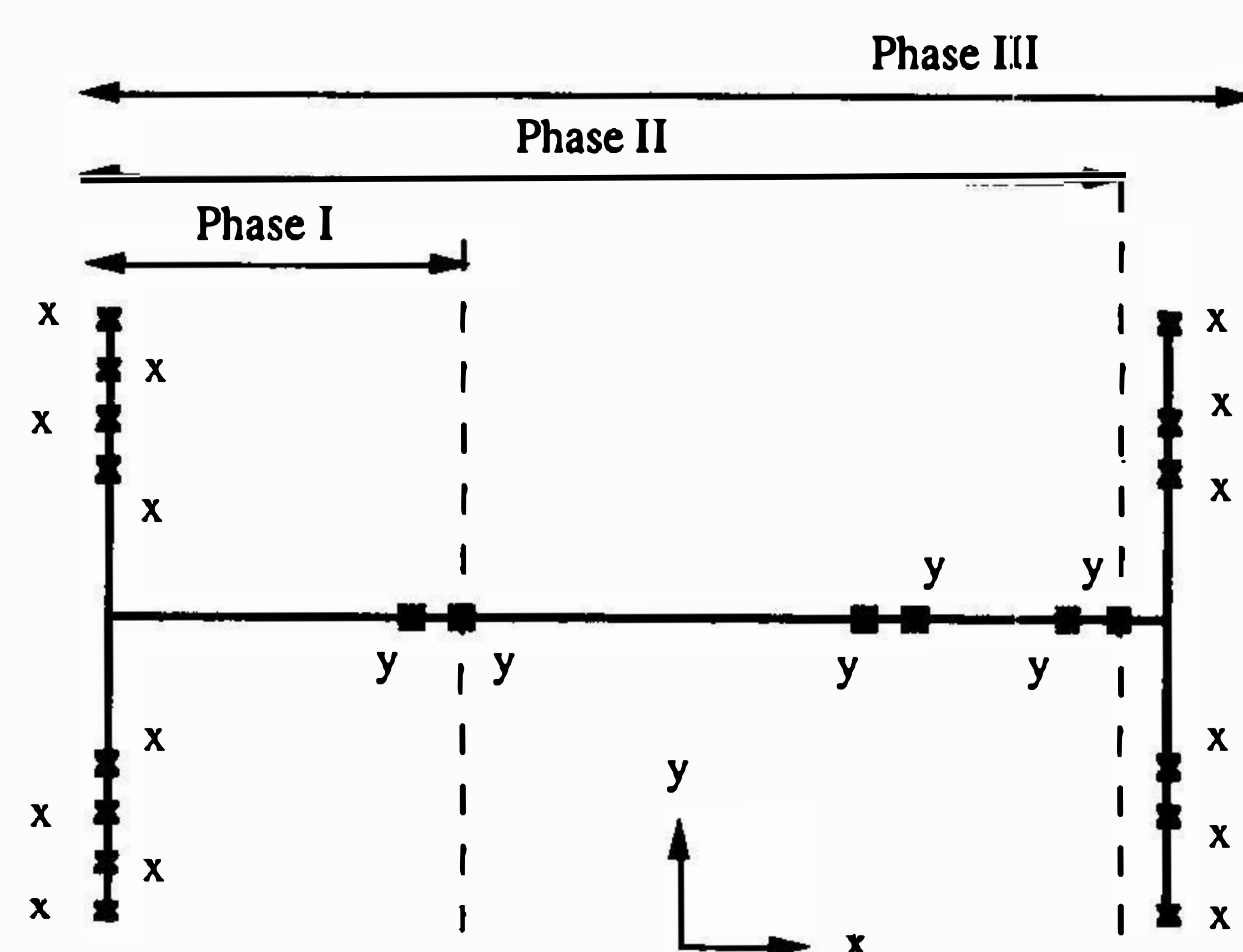


Fig. 6 Sensor configuration for phase-by-phase placement analysis



for the Phase I sensor placement analysis. All 40 degrees of freedom in the Phase I finite element model were included in the initial candidate sensor set. Ten sensors were placed using the Effective Independence technique requiring 30 iterations. Figure 5 shows the Effective Independence value for each sensor in the final configuration. Figure 6 illustrates the selected sensor locations on the Phase I portion of the space structure.

Phase II of the space structure, pictured in Fig. 1, was analyzed in the same manner. Fixed interface modes were computed after constraining the actuator locations, 108 and 118 in the y directions, and the degrees of freedom at the interface to the structure to be added in the next phase, node 121 in the x and y directions, as illustrated in Fig. 7. The effective excitation mass was then computed for the fixed interface modes. Table 3 lists the ten most important Phase II fixed interface mode shapes. The cumulative sum indicates that retaining eight modes will produce a Craig-Bampton representation which will accurately predict 95% of the Phase II dynamics affected by the actuator/interface inputs. The reduced Craig-Bampton representation was produced using a transformation matrix consisting of the eight identified fixed interface modes and four excitation constraint modes. A modal solution was performed producing twelve mode shapes in the Craig-Bampton space. Transforming these modes to the finite element configuration space and performing a cross-orthogonality computation identified ten finite element model mode shapes which were accurately predicted by the reduced Craig-Bampton representation. The cross-generalized mass values and the corresponding frequency errors are listed in Table 4. These ten modes will be strongly affected by the actuator/interface inputs.

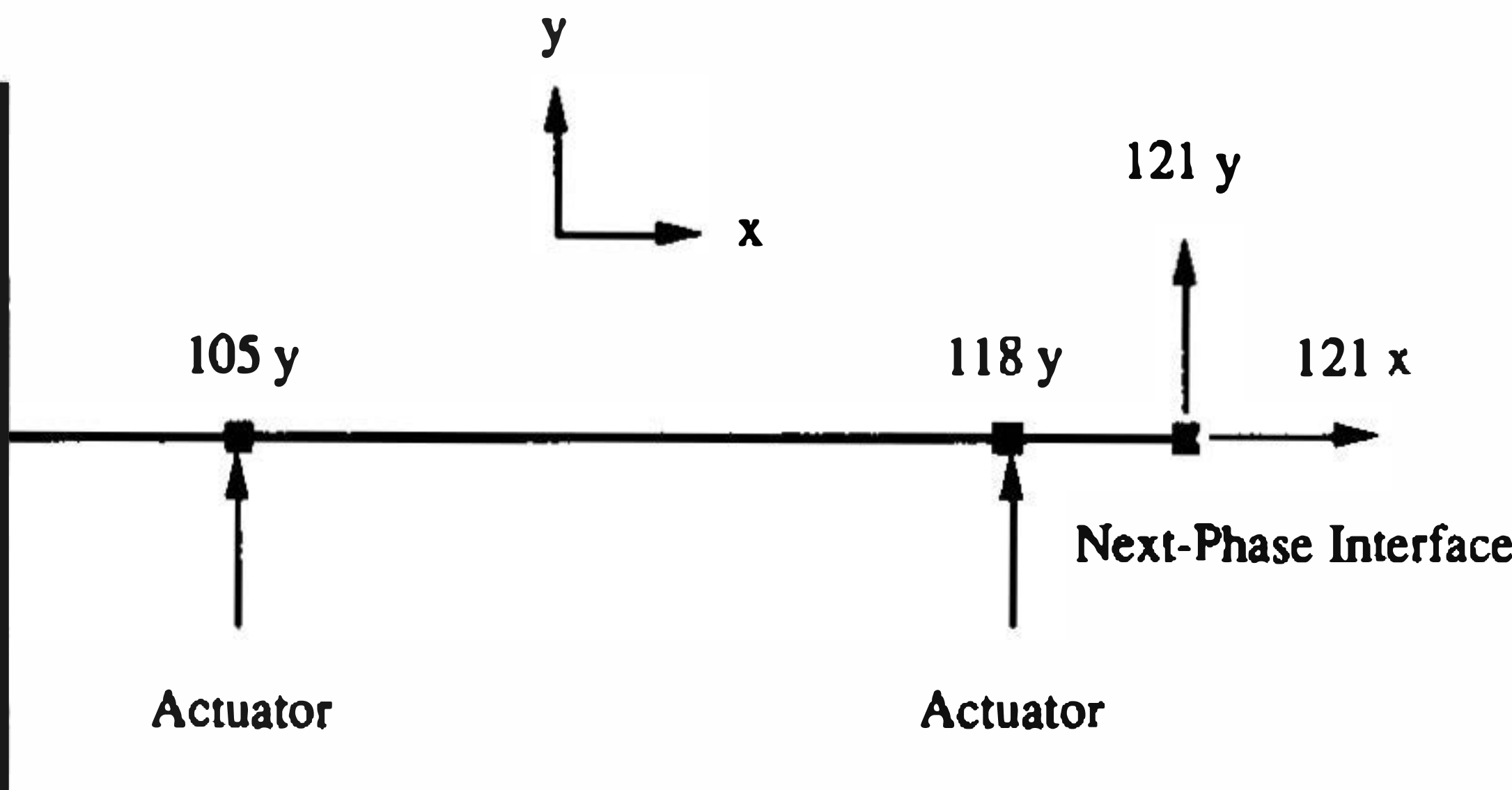


Fig. 7 a-set degrees of freedom for Phase II

TABLE 3 TEN MOST IMPORTANT PHASE II FIXED INTERFACE MODES BASED ON EFFECTIVE EXCITATION MASS

Mode	Freq. (Hz)	Eff. Mass	Cummulative Eff. Mass
3	0.213	0.373	0.373
24	20.765	0.173	0.546
1	0.072	0.139	0.685
4	0.469	0.129	0.814
6	0.514	0.067	0.881
2	0.076	0.040	0.920
9	2.408	0.012	0.933
5	0.500	0.012	0.945
36	55.779	0.006	0.951
45	131.870	0.005	0.956

TABLE 4 FINITE ELEMENT MODEL/CRAIG-BAMPTON REPRESENTATION CORRELATION RESULTS FOR PHASE II

FEM Mode	Freq. (Hz)	CB Mode	Freq. (Hz)	Absolute % Error	CGM
1	0.000	1	0.000	0.000	1.00
2	0.000	2	0.000	0.000	1.00
3	0.000	3	0.000	0.000	1.00
4	0.077	4	0.077	0.000	1.00
5	0.083	5	0.083	0.001	1.00
6	0.275	6	0.275	0.011	1.00
7	0.491	7	0.491	0.001	1.00
8	0.514	8	0.514	0.009	1.00
9	0.998	9	1.004	0.652	1.00
12	1.882	10	1.933	2.703	0.98
15	3.462	11	3.802	9.824	0.87
35	48.271	12	55.243	14.442	0.72



The seven elastic finite element mode shapes predicted by the Craig-Bampton representation were used as target modes for sensor placement in Phase II. Fourteen sensors were placed to identify the target modes. The initial candidate sensor set consisted of the ten sensor locations selected in Phase I and all the additional finite element model node degrees of freedom added in the new structure corresponding to Phase II. Twenty two iterations were performed to determine the 14 best sensor locations. However, none of the Phase I locations could be deleted from the candidate set. Therefore, the four best additional sensors were selected from the new portion of the structure to augment the Phase I sensor locations. The sensor locations for Phase II are illustrated in Fig. 6.

A modal solution of the full unconstrained space structure produced 30 mode shapes with frequencies below 7.6 Hz. The first 10 frequencies are listed in Table 5. A typical mode shape is illustrated in Fig. 8. Fixed interface modes were computed by fixing the two actuator location degrees of freedom, 108y and 118y. The fixed interface modal frequencies are also presented in Table 5. Note that there is one zero frequency rigid body mode present due to the fact that the actuators cannot control or excite rigid body translation in the x direction. Table 6 lists the top ten fixed mode shapes based on effective excitation mass. Though not listed, the rigid body mode possessed zero effective excitation mass, as expected. Retaining eight fixed interface mode shapes provides 95% structural completeness relative to the actuator inputs. Due to the presence of the rigid body mode in the fixed interface mode set,  $[K_{oo}]$  is singular and thus the alternate formulation of Eq. (9) must be used to compute the excitation constraint modes.

The finite element model target modes for the full structure were then identified by computing the modal parameters of the reduced Craig-Bampton representation and performing a cross-orthogonality

**TABLE 5 FULL SPACE STRUCTURE UNCONSTRAINED AND FIXED INTERFACE MODAL FREQUENCIES**

Mode	Free Freq. (Hz)	Fixed Freq. (Hz)
1	0.000	0.000
2	0.000	0.069
3	0.000	0.073
4	0.070	0.076
5	0.076	0.087
6	0.077	0.162
7	0.087	0.265
8	0.169	0.475
9	0.482	0.500
10	0.493	0.502

**TABLE 6 TEN MOST IMPORTANT PHASE III FIXED INTERFACE MODES BASED ON EFFECTIVE EXCITATION MASS**

Mode	Freq. (Hz)	Eff. Mass	Cummulative Eff. Mass
7	0.265	0.487	0.487
12	0.528	0.188	0.674
8	0.475	0.113	0.788
3	0.073	0.076	0.864
6	0.162	0.037	0.901
17	2.368	0.022	0.923
33	8.671	0.013	0.935
28	6.791	0.012	0.947
10	0.502	0.012	0.960
36	11.765	0.007	0.965

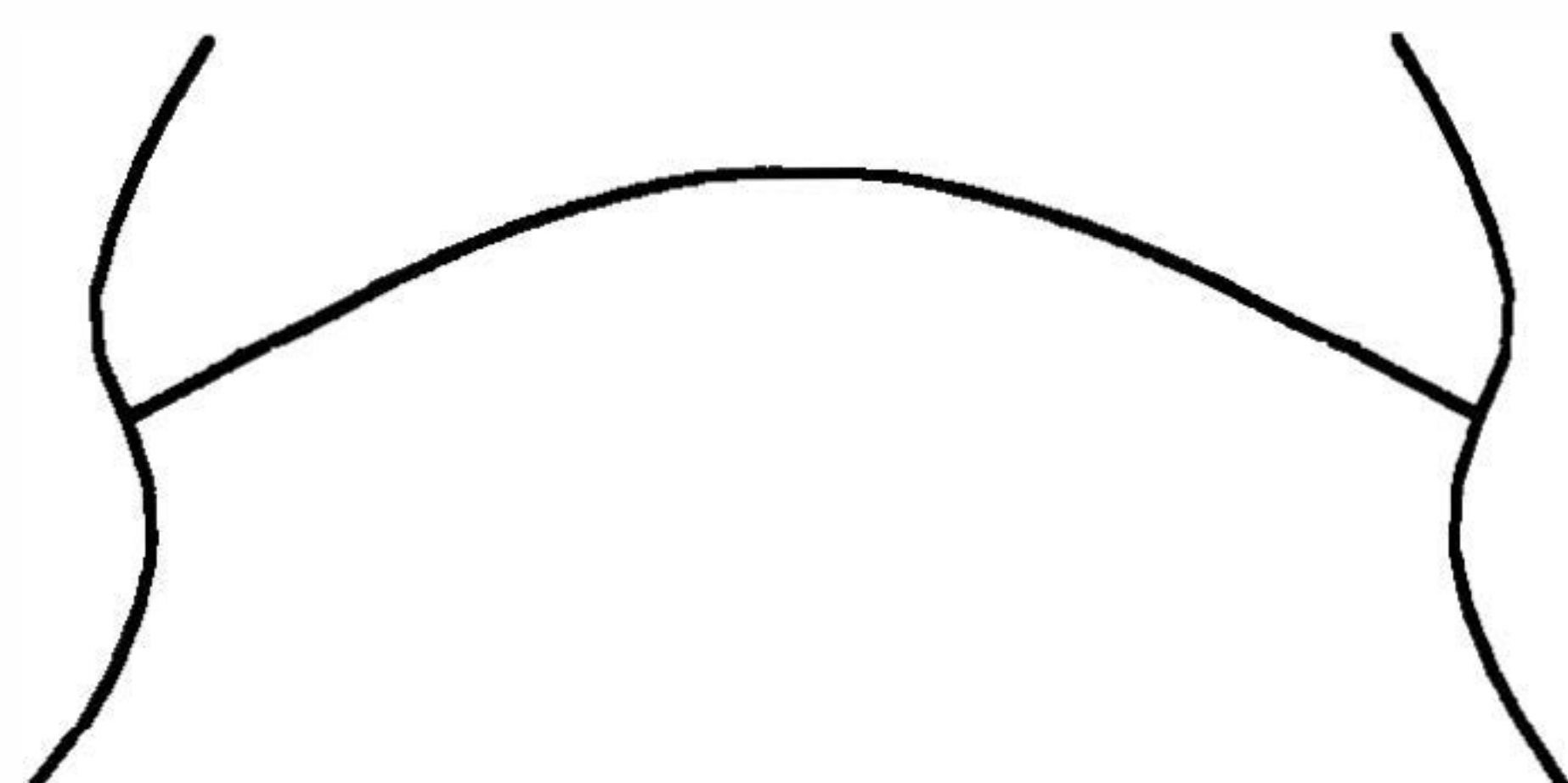


**Fig. 8 Typical space structure elastic mode shape-mode 8 (0.169 Hz)**



computation with respect to the finite element model modes. The results listed in Table 7 indicate that seven modes and frequencies were accurately predicted by the Craig-Bampton representation. The five elastic modes were used as target modes for sensor placement. These five mode shapes will be strongly excited by the actuator inputs during an on-orbit modal survey. The Effective Independence technique was used to place an additional six sensors on the new structure added in the final phase while retaining the 14 sensors placed in Phases I and II. The additional sensor locations are illustrated in Fig. 6.

In order to measure the effectiveness of the phase-by-phase sensor placement approach presented in this paper, it was compared with the optimal sensor configuration for the full space structure. Using Effective Independence, the 20 best sensors were iteratively selected from an initial candidate set including all 92 full structure finite element model degrees of freedom using the five elastic target modes excited by the actuators. The resulting sensor configuration is illustrated in Fig. 9. The straightforward approach to phase-by-phase modal identification would be to place the sensors on each phase based upon what was optimally predicted for the full structure. Modal identification of each phase would then be based upon a subset of the optimal sensor configuration. The full structure optimal sensor set provided eight sensors for Phase I, and 14 sensors for Phase II.

The goodness of a sensor configuration was measured at each phase by the determinant and condition

**TABLE 7 FINITE ELEMENT MODEL/CRAIG-BAMPTON REPRESENTATION CORRELATION RESULTS FOR FULL SPACE STRUCTURE**

FEM Mode	Freq. (Hz)	CB Mode	Freq. (Hz)	Absolute % Error	CGM
1	0.000	1	0.000	0.000	1.00
2	0.000	2	0.000	0.000	1.00
6	0.077	3	0.077	0.038	1.00
8	0.169	4	0.169	0.045	1.00
9	0.482	5	0.482	0.045	1.00
10	0.493	6	0.493	0.029	1.00
13	0.810	7	0.813	0.308	1.00
14	1.309	8	1.355	3.481	0.84
23	3.087	9	2.973	3.683	0.74
29	6.459	11	10.591	63.979	0.61
30	7.595	10	7.835	3.153	0.36

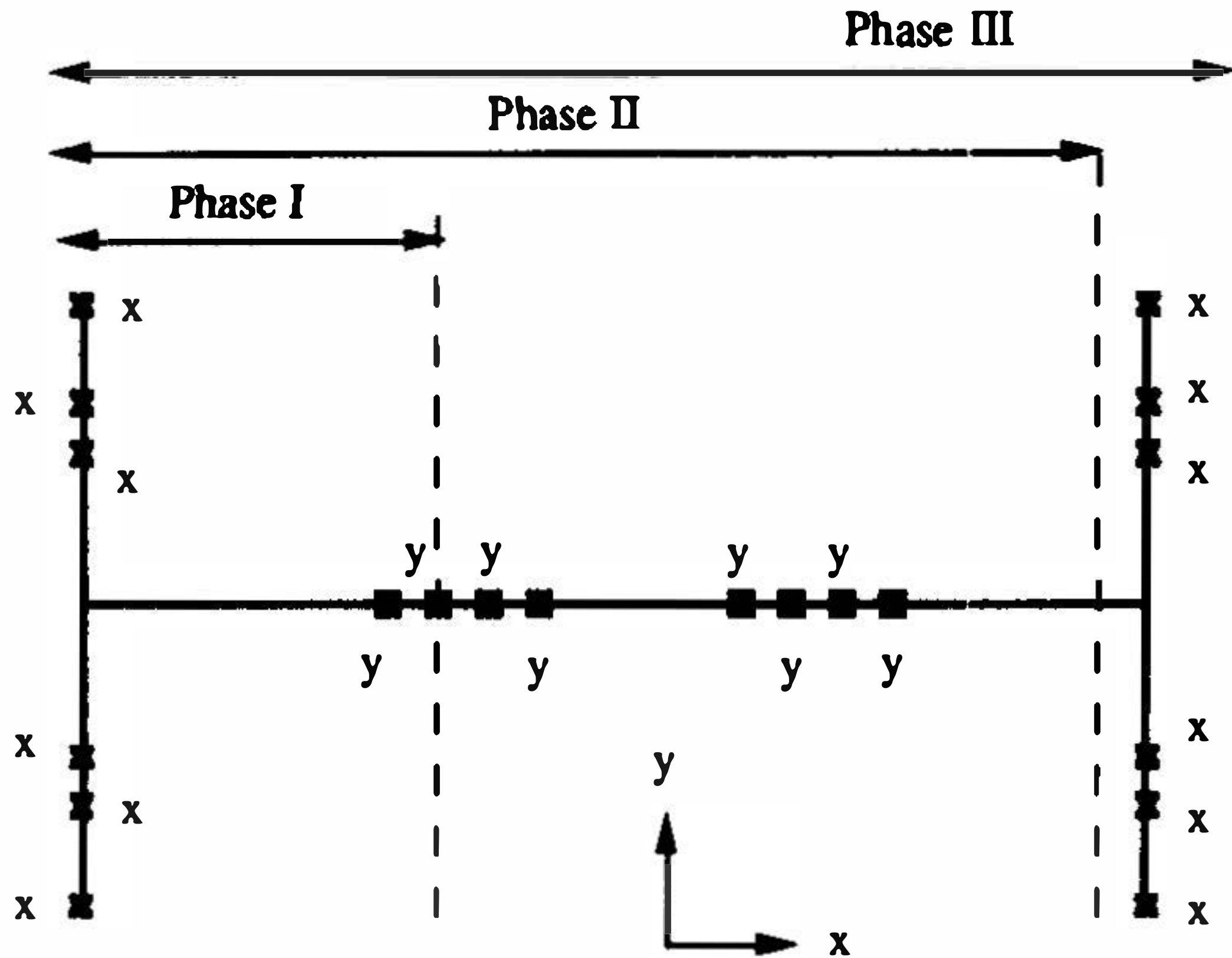


**Fig. 9 Optimal sensor placement for full structure using 5 elastic target modes**

**TABLE 8 FISHER INFORMATION MATRIX MEASURES BY PHASE FOR SEQUENTIALLY PLACED SENSORS AND SUBSETS OF OPTIMAL SENSORS**

	Phase I		Phase II		Phase III	
	Det	Cond	Det	Cond	Det	Cond
Sequential	1.060e2	1.032	1.524e4	5.954	3.825e3	13.206
Subset	9.280e1	1.181	1.046e3	22.206	8.976e3	6.527



number of the information matrix produced using modes which are strongly excited by the current-phase actuators. Only these modes will actually be excited during a modal survey of any particular phase. They are a subset of the target modes used to place sensors in the phase-by-phase analysis. In Phase I, the actuator will excite modes 5 and 6, while in Phase II, the two actuators will excite modes 4, 6, 7, 9, and 12. This can be determined by regenerating the Phase I and Phase II Craig-Bampton representations and retaining only fixed interface modes which contribute significantly to the effective mass in each column of the effective mass matrix of Eq. (11) corresponding to an actuator location. The final phase target modes are those already identified in Table 7.

Table 8 lists the information matrix determinant and condition number by space structure phase for the sensor configurations derived by the phase-by-phase analysis and optimal placement based on the full structure. The determinant is a measure of the amount of information in the sensor data pertaining to the target modes while the condition number is a measure of their spatial independence. A value of 1.0 would indicate orthogonality. In the first Phase, the phase-by-phase placed sensors slightly outperform the sensor set placed using the full structure. Sensors were placed in Phase I to not only identify modes excited by the actuators, but also to identify modes which will be excited by inputs at the next-phase interface. Thus in Phase II, the phase-by-phase sensor configuration produces a much larger determinant and a much smaller condition number than the values generated by the Phase II sensor set placed using the full structure. In the final phase, the optimally placed sensors outperform the phase-by-phase sensor configuration as expected, however, the results are comparable.

A method has been presented for target mode identification and sensor placement on a phase-by-phase basis for sequentially assembled large space structures. At each phase, a Craig-Bampton representation was generated by constraining the structure at the actuator locations and at the interface to the next phase. Fixed interface modes were computed and ranked according to dynamical importance using an absolute measure called effective excitation mass. Modes with large excitation mass will be strongly excited by the actuators during a current phase modal survey, or will be strongly excited by inputs from the next-phase structure. Inclusion of fixed interface modes in the Craig-Bampton representation which are strongly excited by the next-phase structure allows sensors placed during the current phase to do a better job of anticipating the dynamics which will be important in the next phase.

Finite element model target modes were identified at each phase by performing cross-orthogonality computations between the finite element model modes and the mode shapes predicted by the corresponding Craig-Bampton representation in which fixed interface modes were retained to 95% effective excitation mass. Finite element model modes which were accurately predicted by the Craig-Bampton representation were used as target modes for sensor placement at each phase. The sensor configurations placed using the proposed method provided superior information matrix determinants and condition numbers for both Phases I and II when compared to results using subsets of the sensor set placed optimally for the full structure. As expected, the optimal sensor set provided the best results for the final phase, but the sequentially placed sensor set also provided adequate results. It is believed that the proposed method of sensor placement will in general provide sensor configurations that will allow more accurate phase-by-phase modal identification using less sensor resources.

1. Chen, J.C.; Garba, J. A. "Structural analysis model validation using modal test data." *Joint ASCE/ASME Mechanics Conference*, Albuquerque, NM, 1985. p 109-137



2. Kammer, D. C.; Jensen, B. M.; Mason, D. R. "Test-analysis correlation of the space shuttle solid rocket motor center segment." *J Spacecr Rockets* v 26 n 4 p 266-273 1989.
3. Kammer, D. C. "An optimum approximation for residual stiffness in linear system identification." *AIAA J* v 6 n 7 p 104-112 1988.
4. Berman A.; Wei, F.; Rao, K. V. "Improvement of analytical dynamic models using modal test data." *21st AIAA Structures, Structural Dynamics, and Materials Conference Papers*, 1980. p 809-814
5. Kabe, A. "Stiffness matrix adjustment using mode data." *AIAA J* v 23 n 9 p 1431-1436 1985.
6. Juang, J. L.; Rodriguez, G. "Formulations and applications of large structure actuator and sensor placements." *2nd VPI&SU/AIAA Symposium on Dynamics and Control of Large Flexible Spacecraft Proceedings*, 1979. p 247-262
7. Baruh, H.; Choe, K. "Sensor placement in structural control." *J Guid Control Dyn* v 13 n 3 p 524-533 1990.
8. Norris, G. A.; Skelton, R. E. "Selection of dynamic sensors and actuators in the control of linear systems." *J Dyn Syst Meas Control Trans ASME* v 111 n 3 p 389-397 Sep 1989.
9. Delorenzo, M. L. "Sensor and actuator selection for large space structure control." *J Guid Control Dyn* v 13 n 2 p 249-257 1990.
10. Shah, P. C.; Udwadia, F. E. "A methodology for optimal sensor locations for identification of dynamic systems." *J Appl Mech* v 45 n 1 p 188-196 Mar 1978.
11. Udwadia, F. E.; Garba, J. A. "Optimal sensor locations for structural identification." *Proceedings of the JPL Workshop on Identification and Control of Flexible Space Structures*, 1985. p 247-261
12. Kammer, D. C. "Sensor placement for on-orbit modal identification and correlation of large space structures." *J Guid Control Dyn* v 14 n 9 p 251-259 1991.
13. Kammer, D. C. "Effect of model error on sensor placement for on-orbit modal identification of large space structures." to be published in *J Guid Control Dyn* v 15 n 2 p 334-341 Mar/Apr 1992.
14. Kammer, D. C., "Effects of noise on sensor placement for on-orbit modal identification of large space structures." to be published in *J Dyn Syst Meas Control Trans ASME*
15. Lim, T. W. "Sensor placement for on-orbit modal testing." *AIAA/ASME/ASCE/AHS 32nd Structures, Structural Dynamics, and Materials Conference Papers*, Baltimore, MD, 1991. p 2977-2985
16. Kammer, D. C.; Yao, L. "Application on effective independence to sensor placement for identification of a space station photovoltaic array." submitted to *J Sound Vib*
17. Moore, B. C. "Principal component analysis in linear systems: controllability, observability, and model reduction." *IEEE Trans Automatic Control* v AC-26 n 1 p 17-32 Feb 1981.
18. Kabamba, P. T. "Model reduction by Euclidean methods." *J Guid Control* v 3 n 6 p 555-562 1979.
19. Skelton, R. E.; Hughes, P. C. "Modal cost analysis for linear matrix-second-order systems." *J Dyn Syst Meas Control Trans ASME* v 102 p 151-158 1980.
20. Clough, R. W.; Penzien, J. *Dynamics of Structures*. New York: McGraw-Hill; 1975. p 546-578
21. Craig, R. R., Jr.; Bampton, M. C. C. "Coupling of substructures for dynamic analysis." *AIAA J* v 6 n 7 p 1313-1319 1968.
22. Ben-Israel, A.; Greville, T. N. E. *Generalized Inverses: Theory and Application*. New York: John Wiley and Sons; 1974.
23. Rubin, S. "An improved component-mode representation." *AIAA/ASME/SAE 15th Structures, Structural Dynamics, and Materials Conference*, Las Vegas, NV, 1974. Paper # 74-386
24. Ohkami, Y.; and Likins, P. "The influence of spacecraft flexibility on system controllability and observability." *IFAC*, USSR, 1974
25. Linkins, P.; Ohkami, Y.; Wong, C. "Appendage modal coordinate truncation criteria in hybrid coordinate dynamic analysis." *J Spacecr Rockets* v 13 n 10 p 611-617 1976.
26. Hughes, P. C.; Skelton, R. E. "Controllability and observability of linear matrix-second-order systems." *J Appl Mech* v 47 n 2 p 415-420 Jun 1980.
27. Schweppe, F. C. *Uncertain Dynamic Systems*. Englewood Cliffs, NJ: Prentice-Hall; 1973.
28. Middleton, D. *An Introduction to Statistical Communication Theory*. New York, NY: McGraw-Hill; 1960.
29. Fedorov, V. V. *Theory of Optimal Experiments*. New York, NY: Academic Press; 1972.





**HYATT ORLANDO HOTEL**  
Kissimmee, FL  
February 1-4, 1993

Sponsored by

**UNION COLLEGE**  
and  
**SOCIETY FOR EXPERIMENTAL  
MECHANICS, INC.**

**Abstract deadline: June 5, 1992**

**INQUIRIES:** Director, Dominick J. DeMichele, (518) 346-3650

Asst. Director, Kenneth A. Galione;  
Conference Manager, Katherine M. Ramsay;  
Exhibit Sales Coordinator, Kathryn J. Richter;

Society for Experimental Mechanics, Inc.  
7 School Street, Bethel, CT 06801  
Phone: (203) 790-6373; FAX (203) 790-4472